Clinical Progress

Cell Stem Cell

Human Embryonic Stem Cell-Derived Oligodendrocyte Progenitors Remyelinate the Brain and Rescue Behavioral Deficits following Radiation

Graphical Abstract

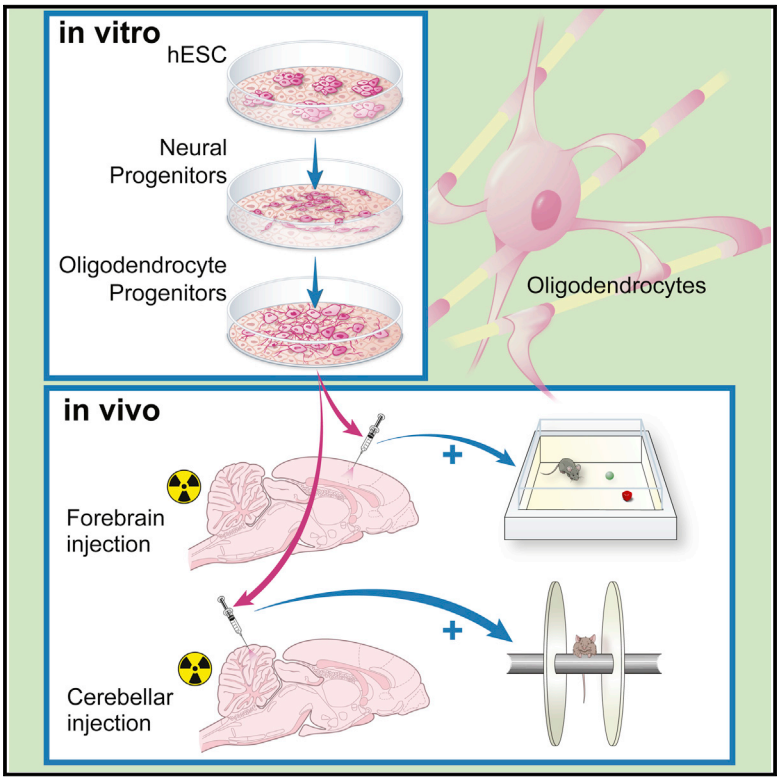

Authors

Jinghua Piao, Tamara Major, ..., Denis Soulet, Viviane Tabar

Correspondence

tabarv@mskcc.org

In Brief

Radiation injury to the brain remains a common problem among cancer survivors, leading to significant deterioration in quality of life. A key long-term consequence of radiation is diffuse demyelination. Piao et al. derive oligodendrocyte progenitors from hPSCs and demonstrate that engrafted cells restore myelination and behavioral defects of irradiated rats.

Highlights

- A clinical dose of brain radiation induces demyelination and behavioral deficits
- Oligodendrocyte progenitors (hOPC) are derived from human pluripotent stem cells
- hOPCs grafted in the forebrain remyelinate the brain and rescue cognitive deficits
- hOPC grafts in the cerebellum are required for improvement in motor tasks

Piao et al., 2015, Cell Stem Cell *16*, 198–210
February 5, 2015
http://dx.doi.org/10.1016/j.stem.2015.01.004

CellPress

Cell Stem Cell
Clinical Progress

Human Embryonic Stem Cell-Derived Oligodendrocyte Progenitors Remyelinate the Brain and Rescue Behavioral Deficits following Radiation

Jinghua Piao,[1,6] Tamara Major,[1,6] Gordon Auyeung,[1] Edelweiss Policarpio,[1] Jayanthi Menon,[1] Leif Droms,[1] Philip Gutin,[1] Kunihiro Uryu,[3] Jason Tchieu,[2] Denis Soulet,[4,5] and Viviane Tabar[1,*]

[1]Department of Neurosurgery and Center for Stem Cell Biology, Memorial Sloan Kettering Cancer Center, New York, NY, 10065, USA
[2]Developmental Biology Program, Sloan Kettering Institute, New York, NY 10065, USA
[3]Resource Center (EMRC), The Rockefeller University, New York, NY 10065, USA
[4]Department of Psychiatry and Neuroscience, Faculty of Medicine, Laval University, QC, Canada, G1V 0A6
[5]Axe Neuroscience, Centre de recherche du CHU de Québec, QC, Canada, G1V 0A6
[6]Co-first author
*Correspondence: tabarv@mskcc.org
http://dx.doi.org/10.1016/j.stem.2015.01.004

SUMMARY

Radiation therapy to the brain is a powerful tool in the management of many cancers, but it is associated with significant and irreversible long-term side effects, including cognitive decline and impairment of motor coordination. Depletion of oligodendrocyte progenitors and demyelination are major pathological features that are particularly pronounced in younger individuals and severely limit therapeutic options. Here we tested whether human ESC-derived oligodendrocytes can functionally remyelinate the irradiated brain using a rat model. We demonstrate the efficient derivation and prospective isolation of human oligodendrocyte progenitors, which, upon transplantation, migrate throughout the major white matter tracts resulting in both structural and functional repair. Behavioral testing showed complete recovery of cognitive function while additional recovery from motor deficits required concomitant transplantation into the cerebellum. The ability to repair radiation-induced damage to the brain could dramatically improve the outlook for cancer survivors and enable more effective use of radiation therapies, especially in children.

INTRODUCTION

The ability to direct pluripotent stem cells (hPSC) into specific fates has raised hopes of translating these efforts into effective therapies. There has been notable progress in the neural field, where several therapeutically relevant cell types have been derived using greatly improved and highly reproducible protocols (Tabar and Studer, 2014). The derivation of engraftable glia has also been reported and the most recent studies have convincingly demonstrated the ability of human pluripotent stem-cell-derived oligodendrocytes to achieve extensive myelination in vivo following transplantation into neonatal *Shiverer* mice (Hu et al., 2009, Wang et al., 2013; Douvaras et al. 2014). These are promising data, though oligodendrocyte differentiation protocols remain complex and protracted, and applications have not been tested much beyond this genetic neonatal model.

Here, we present a novel indication for human PSC-derived oligodendrocytes, namely the repair of diffuse demyelination occurring as a consequence of radiation injury to the brain, a clinically important but largely unmet need among cancer survivors. Radiation therapy to the brain is a commonly prescribed treatment for many cancers, including primary and metastatic brain tumors, as well as in prophylactic regimens in small cell cancers (Paumier et al., 2011) or leukemia (Gibbs et al., 2006). It is often associated with significant long-term cognitive symptoms, even at standard doses and using modern techniques (Greene-Schloesser et al., 2012). Progressive impairments in memory, attention, executive function, and motor coordination are described, as well as learning difficulties and a decrease in intelligence quotients (IQ) in children (Schatz et al., 2000). The clinical course is often progressive and irreversible, and there is no effective treatment for radiation-induced cognitive decline. Nevertheless, the use of high volume CNS radiation continues to be a therapeutic cornerstone in many cancers, for palliative or curative purposes (Ringborg et al., 2003). The pathogenesis of the late effects (months to years) of radiation is not completely understood, and studies in animals and humans support an important role for the depletion of the oligodendrocyte precursor pool and subsequent demyelination (Kurita et al., 2001; Oi et al., 1990; Panagiotakos et al., 2007). In addition to autopsy data, there is increasing evidence from recent diffusion tensor imaging studies that support the premise that radiation results in early and progressive damage to the white matter and that the latter's integrity correlates with intellectual outcome (Mabbott et al., 2006; Uh et al., 2013). Other areas of potential injury include the vascular compartment, whereby thrombosis and hyalinization can be seen subacutely, particularly following high doses of radiation (Duffner et al., 1985), as well as the subventricular zone (SVZ) and hippocampus where transit amplifying and/or neural stem cells reside (Monje et al., 2002, 2003). However, it is evident that the plethora of radiation-related symptoms cannot

be solely attributed to the disruption of neurogenesis in the hippocampus and the SVZ, especially in humans. Data from our lab and others demonstrate that radiation extensively targets the large pool of mitotically active oligodendrocyte progenitors. These cells are acutely reduced in number and eventually depleted, followed by progressive, often patchy, demyelination (Sano et al., 2000; Panagiotakos et al., 2007). Here, we model the effects of radiation in young rats, using a clinically relevant fractionated regimen of 50 Gy to the whole brain. Our data show depletion of the oligodendrocyte pool and a delayed onset of demyelination, as well as cognitive and motor deficits. Concomitantly, we optimize a protocol for the derivation and selective enrichment of late oligodendrocyte progenitors (O4-expressing) from human embryonic stem cells (ESCs) and demonstrate that these cells can remyelinate the brain and ameliorate behavioral deficits. The clinical impact of these studies can be substantial as the need to address quality of life in cancer survivors grows more pressing.

RESULTS

Impact of Radiation on the Young Rat Brain

We subjected 4-week-old Sprague-Dawley rats to a dose of 50 Gy of radiation, administered in 10 fractions to the whole brain. Analysis of the brains at 14 weeks demonstrated a significant decrease in the number of oligodendrocyte progenitors throughout the brain as determined by the number of oligodendrocyte transcription factor 2 (olig2)-expressing cells and the decrease in O4 expression (Figure 1A; Figure S1A). This was associated with a decrease in myelin basic protein (MBP) expression and in the volume of the corpus callosum by ~25%, as determined by stereological volume analysis. The loss of MBP encompassed all major white matter pathways including the corpus callosum, the hippocampal fimbria, the commissures, as well as the subcortical areas and the cerebellum (Figure 1B; Figure S1A). The irradiated brain showed mild evidence of an inflammatory response demonstrated by an increase in the number of activated microglial/macrophages (ED1/Iba-1), and no significant gliosis at 14 weeks after radiation (Figure S1B). Behavioral testing was conducted on the irradiated and the normal age-matched groups. It consisted of cognitive and memory tests, including novel object preference and object location tasks, as well as water maze and rotarod testing with acceleration conditions. The data showed a significant decline in performance on the novel object preference and object location tasks (Barker et al., 2007), as well as a decrease in the duration of time spent on the rotarod wheel (from 11.8 to 2.2 s) and a substantial decrease in the distance traversed during that test (from ~1 m to 0.18 m) (Figures 1C and 1D). The water maze task did not result in a statistically significant difference in either the time spent or distance traveled in the target quadrant in probe test, as previously reported (Saxe et al., 2006; Vorhees and Williams, 2006) (Figure S1C).

Derivation of Late Oligodendrocyte Progenitors from Human Embryonic Stem Cells

Recent advances in the field of human pluripotent stem cell biology have led to highly robust protocols for neural differentiation and specification into various neural and non-neural fates. However, the oligodendrocyte lineage has been a long-standing challenge in the field, due to the requirement for lengthy in vitro differentiation periods (Wang et al., 2013; Douvaras et al. 2014), perhaps compatible with the protracted developmental timeline followed in utero. We optimized a human pluripotent stem cell protocol that allows the derivation of well characterized oligodendrocyte progenitors by 70 days in vitro (DIV) through several stages, including neural induction, patterning of neural precursors, oligodendrocyte progenitor proliferation, and differentiation (Figure 1E). Undifferentiated hESCs were subjected to neural induction by dual SMAD and Wnt/β-catenin inhibition using LDN193189 (LDN), SB431542 (SB), and XAV939 (XAV) (Chambers et al., 2009), resulting in the emergence of ZO-1/LIN-28/Nestin-expressing CNS neural rosettes. Neural precursors emerging from rosettes express Pax6 and FOXG1, suggesting an anterior forebrain identity; they are replated in the presence of purmorphamine, a smoothened agonist that activates the hedgehog pathway. Cells are then passaged in the presence of FGF8, and on DIV 40, they are exposed to glial media containing PDGFRα, IGF-1, cAMP, and T3. Early oligodendrocyte progenitors are observed in the culture on day 45 and are characterized by NKx2.2/Olig2/PDGFRα expression (Figure 1F). PDGFRα$^+$ progenitors are highly proliferative (Ki-67 of 57%) and co-label for Sox10 (Figures S1D and S1E). Their proportion in the culture increases steadily from an average of 6% to 25% on DIV 100 (Figures S1F and S1G). Late oligodendrocyte progenitors (O4-expressing) emerge by DIV 50, increasing steadily to ~35% by DIV 100, while maintaining expression of Olig2, Nkx2.2, and Sox10 (Figure 1F; Figures S2A and S2B). These cells mature in overlapping waves, leading to the gradual appearance of oligodendrocytes that express O1 and MBP. Further in vitro maturation of the majority of the cells (>85%) is achieved by exposure to differentiation media (BDNF, AA, T3, and cAMP) for 2 weeks, leading to morphologically mature oligodendrocytes that express O1, myelin-associated glycoproteins such as MOG and MAG, and MBP (Figure 1G). FACS sorting for late oligodendrocyte progenitors (O4 expressing) (Figure S2C) leads to highly enriched cultures with >93% of cells expressing O4 (remaining cells are olig2$^+$, data not shown) and co-labeling for Olig2 and Nkx2.2; the majority of those cells are post-mitotic (Ki-67 of 3%) (Figure S2B). Efficient sorting can be performed on DIV 70 or later.

We further characterized the O4$^+$ sorted cells by global transcriptomal analysis (Figures S2D and S2E). Comparison of the expression profile of O4-enriched day 70 cells with that of undifferentiated H9 ESCs, showed the robust induction of transcription factors related to oligodendrocyte identity such as *OLIG1*, *OLIG2*, and *SOX10*, *Nkx2.2*, as well significant expression of myelin-related genes *MAG*, *OMG*, and *MBP*. A telencephalic identity was suggested by the upregulation of *FOXG1*, *OTX1*, *EMX2*, and *LHX2* forebrain markers and the absence of *Hox* genes (Figure 1H). RTqPCR (Figure 1I) further validated >10^4-fold change in transcription factors that are master regulators of the oligodendrocyte fate. Functional annotation of enriched gene sets was also compatible with glial and oligodendroglial development (Figure S2F).

To verify the reproducibility of the protocol for oligodendrocyte differentiation, we tested an additional hES line, WA-07 and two iPSC lines, J1 and J2. The iPSC lines were derived from

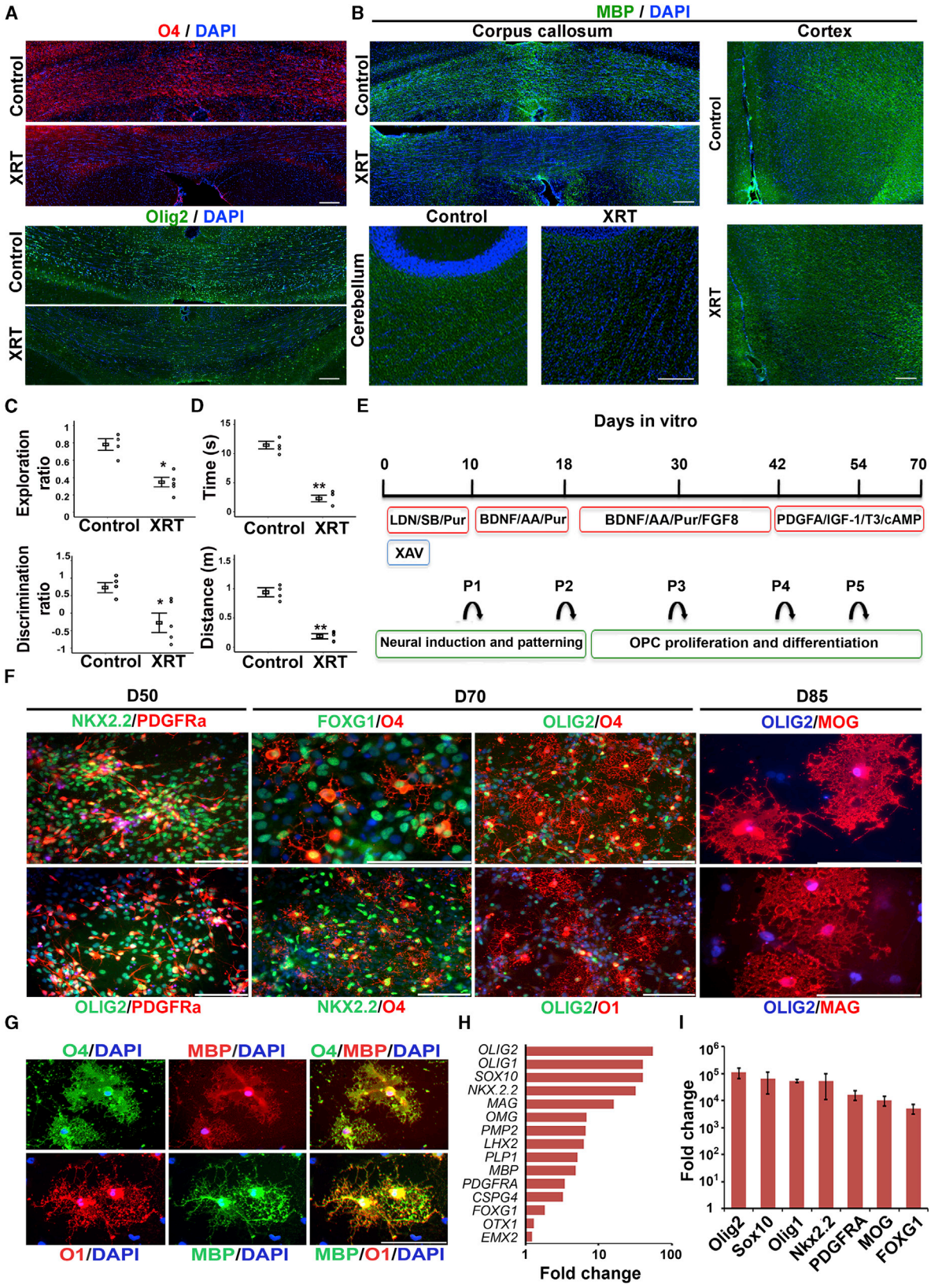

(legend on next page)

fibroblasts of a healthy young donor (J1) and an old donor (J2), and were reprogrammed using Sendai vectors (Miller et al., 2013). All tested lines were capable of oligodendrocyte derivation using the same protocol. Enrichment for $O4^+$ cells on DIV 70 shows a range of 10%–20% $O4^+$ OPC in the cultures. The sorted cells from all three additional lines (H7, J1, and J2) expressed appropriate OPC markers (Olig2, Nkx2.2, Sox10), and exhibited a similar pattern of differentiation and expression of mature markers, e.g., MBP (Figures 2A and 2B). Evidence for myelination of axons was assessed in co-cultures of $O4^+$ OPCs derived from each of the 2 hES and 2 iPSC lines, with human ES-derived neurons or young rat hippocampal neurons (Figure 2C; Figure S3A). After 5 weeks in vitro, the cultures exhibited myelin sheaths along the axons (identified by SMI 312 immunoreactivity); the length of ensheathed/myelinated axons per oligodendrocyte was quantified and found to be similar across the four pluripotent cell lines (Figure 2D). Electron microscopy sections demonstrated the presence of compact myelin sheaths with dense lines (Figure 2E). The cultures did not exhibit any spontaneous or endogenous myelination under control conditions (Figure S3B).

Grafted Human ESC-Derived Oligodendrocytes Remyelinate the Irradiated Brain and Ameliorate Cognitive Function

We then asked whether the human ESC-derived oligodendrocytes could succeed in restoring myelination in the irradiated brains. We thus irradiated a set of 10 nude rats using the same regimen of 50 Gy in 10 fractions, followed by behavioral testing for novel object preference, object location recognition, and rotarod (with acceleration) performance. At 4 weeks post-radiation, the rats (XRT+ graft group) received bilateral stereotactic injections of human ESC-derived oligodendrocytes into the corpus callosum (2 injections per cerebral hemisphere, for a total of 1 million cells). The injected cells were enriched for O4 expression via FACS on DIV 100 (35.7% ± 10.62 of the cells were $O4^+$ pre-sort), immediately prior to grafting. Control groups consisted of non-irradiated animals (control group) and sham injections of Hanks' balanced salt solution (HBSS) into irradiated (XRT group) rats.

Serial behavioral testing was performed on all animals. It consisted of the novel object preference and object location tasks, as well as rotarod testing. While the XRT group continued to exhibit poor performance compared to age-matched normal rats, the irradiated but grafted group demonstrated statistically significant improvements in novel object preference and object location recognition parameters, at 10 weeks after transplantation (Figures 3A and 3B). These tasks reflect multiple cognitive processes related to memory and learning such as preference for novelty and recognition memory (Antunes and Biala, 2012; Barker et al., 2007). However, the animals did not show any improvement in the rotarod task, which involves a challenge to motor balance and coordination (Figure 3C).

Analysis of the grafted brains demonstrated excellent survival of the human cells, which were identified by immunohistochemistry for human nuclear antigen (hNA) or human neural cell adhesion molecule (hNCAM). Cells were found throughout the cerebral hemispheres with many in the corpus callosum where they appeared aligned along the main transverse axis, similar to host cells. Human cells were also distributed along other white matter pathways, including the fimbria of the hippocampus and the commissures, as shown by a series of camera lucida representations and corresponding immunohistochemistry images (Figure 3D). Phenotypic analysis of the surviving human cells by confocal microscopy demonstrated that the majority are oligodendrocytes at various stages of maturity, expressing Olig2, Olig1, O4, myelin-associated glycoprotein (MAG), myelin oligodendrocyte-specific protein (MOSP) (Figures S4A and S4B), and MBP. A detailed analysis of the brain sections demonstrated significant evidence of contribution of the graft cells to remyelination and replenishment of the oligodendrocyte pool. The total number of olig2 cells within the corpus callosum was decreased in the irradiated rats, but replenished to near normal in the grafted animals (control $0.64 \times 10^6 \pm 0.08$; XRT $0.24 \times 10^6 \pm 0.03$; XRT + Graft $0.54 \times 10^6 \pm 0.05$) (Figure 3E). An average of $0.22 \pm 0.01 \times 10^6$ human cells, all expressing olig2, were counted in the corpus callosum and $0.17 \pm 0.05 \times 10^6$ in the hippocampi. These data show that the restoration of olig2 is due in large part to the addition of human cells, rather than the upregulation of olig2 expression in endogenous progenitors. Similarly, a side-by-side comparison of sections from the control, XRT and XRT+ graft brains demonstrates a significant recovery of $O4^+$ progenitors, and evidence of remyelination (Figures 3F and 3G). Imaging-based quantification of the levels of O4 and MBP

Figure 1. Impact of Radiation on the Rat Brain and Derivation of Oligodendrocyte Progenitor Cells from Human Embryonic Stem Cells

(A) Immunohistochemistry shows a decrease in O4 levels and in the number of Olig2+ cells in the corpus callosum in the irradiated (XRT) brain.

(B) A decrease in expression of MBP is noted in various brain regions 14 weeks following radiation compared with normal control.

(C) When compared to age-matched controls (n = 4), irradiated rats (XRT, n = 5) exhibit a decrease in the exploration ratio in the novel object preference task and in the discrimination ratio in the object location task.

(D) The rotarod test also shows a significant decrease in the time spent and the total distance travelled on the accelerating rod.

(E) Schematic protocol for differentiation of human pluripotent stem cells into OPCs.

(F) Immunocytochemical characterization of hES-derived progenitors at progressive stages of differentiation into mature oligodendrocytes. At day 50, early OPCs co-express PDGFRα with Olig2 and Nkx2.2. By day 70, late OPCs emerge, expressing O4 together with Olig2, Nkx2.2, and forebrain specific marker FoxG1. O1 expression also increases as the cells mature; by day 85, they express myelin associated glycoproteins (MOG and MAG).

(G) When placed in differentiation media for 2 weeks, day 70-O4+ cells will mature morphologically and express MBP.

(H) List of selected increased anterior oligospecific genes comparing O4-sorted cell phenotypes versus undifferentiated H9 ESCs, as assessed by microarray analysis.

(I) qRT-PCR analysis of O4 sorted late OPCs at day 70 showed an increase in oligodendrocyte (Olig1, Olig2, Sox10, Nkx2.2, PDGFRα, and MOG) and forebrain-specific markers (FoxG1, OTX1, EMX2) compared to the undifferentiated hES control; $p < 0.01$, n = 3. Fold change is expressed as *log2*.

All panels in (A) and (B) (except for "cerebellum" images) are composites of several low magnification images. All scale bars are 100 μm. Data are mean values ± SEM. (*$p < 0.05$. **$p < 0.01$). Circles in (C) and (D) represent individual scores. All nuclei are counterstained in blue with DAPI. See also Figures S1 and S2.

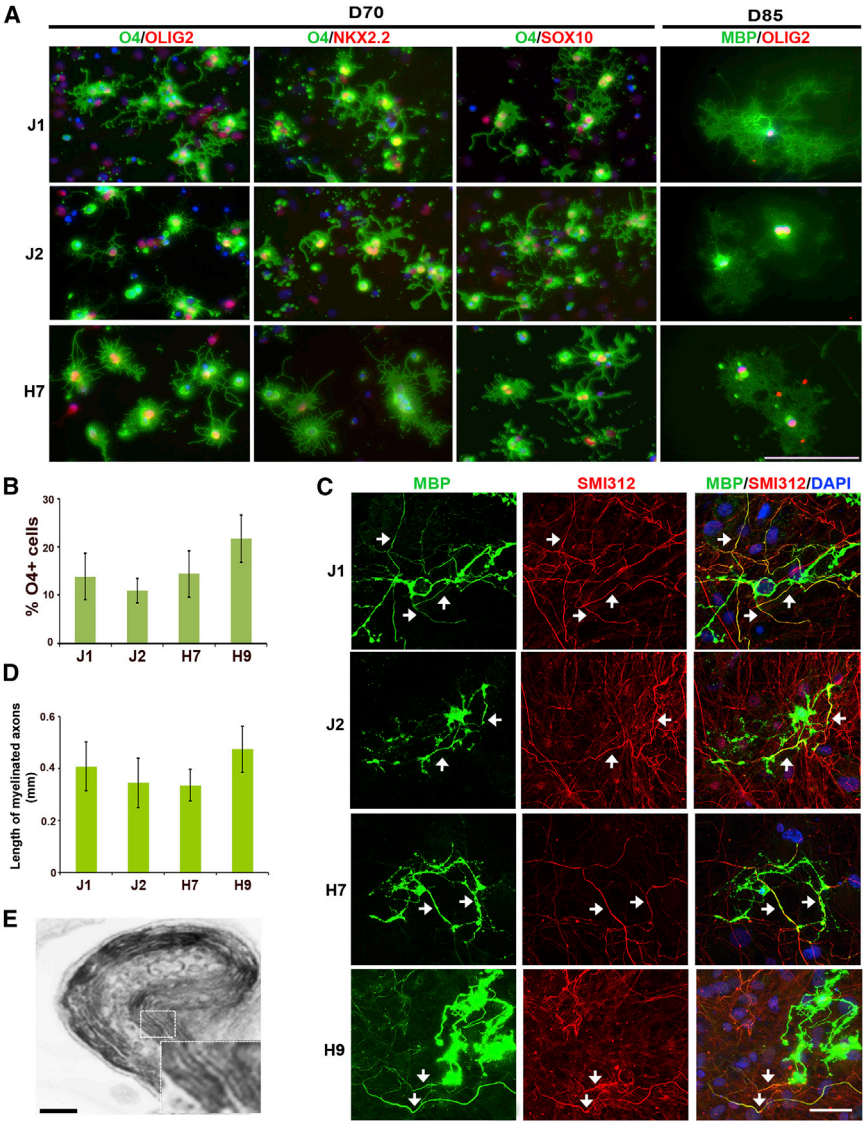

Figure 2. OPCs Can Be Derived from Different Human Pluripotent Stem Cell Lines and Can Myelinate In Vitro

(A) Immunocytochemistry of late OPCs derived from hES line (H7) and 2 iPS lines (J1, J2).The cells co-express Olig2, Nkx2.2, and Sox10 with O4. Day 70 O4+ cells mature into MBP- expressing oligodendrocytes after 2 weeks of differentiation. Scale bar represents 200 μm.

(B) Comparison of the efficiency of OPC derivation by FACS for O4 across four human pluripotent stem cell (hPSC) lines.

(C) In vitro myelination assay: co-culture of O4 sorted cells of different origins with rat hippocampal neurons for 5 weeks. Immunocytochemistry for the axonal marker SMI312 and MBP demonstrates myelination of several axons by a single oligodendrocyte cell. Arrows indicate fibers that co-express both markers. Scale bar represents 50 μm.

(D) Graph represents the total length of axons with myelin sheaths per MBP^+ oligodendrocyte derived from the hPSC lines shown.

(E) Representative electron microscopy (EM) image from a co-culture of OPCs and neurons, showing the formation of multilayered compact myelin sheaths. Scale bar represents 500 nm.

Data are mean values ± SEM. (*$p < 0.05$. **$p < 0.01$). All nuclei are counterstained in blue with DAPI. See also Figure S3, which includes negative control co-cultures.

confirms these observations in a statistically significant manner (Figures 3F and 3G). The decrease in myelin, which followed a patchy pattern, and its recovery are shown in Luxol-stained coronal sections of various areas of the brain (Figure S4C). A stereological volumetric analysis of the corpus callosum also shows recovery to near normal volume in the grafted animals (Figure S4D). We estimated axonal density by immunohistochemistry for SMI312, an axonal marker (Figure S5A), and by electron microscopy and did not note significant differences among the animal groups (axonal density of 149.2 ± 13.55 vs 138.06 ± 11.69 vs 147.15 ± 23.01, per 100 μm^2 in the control, XRT and XRT+ graft groups respectively; $p > 0.05$). Similarly, a stereological estimate of the number of neurons in the cortex did not show changes across the animal groups ($11.71 \pm 1.78 \times 10^6$ in the control vs $11.65 \pm 1.09 \times 10^6$ in the XRT group, Figure S5B). However, the proportion of axons that are ensheathed in myelin shows a significant increase in the grafted animals, compared to the sham treated radiation group (53% ± 6% in the XRT+ graft, vs 27% ± 8% in the XRT and 62% ± 7% in the normal control, Figure 4A). These data suggest that the gain in callosal dimensions is likely due to remyelination and recovery of the glial cell population. MBP, a major component of the myelin sheath is a complex structure that is highly conserved across species (Harauz and Boggs, 2013). In view of their significant homology, MBP of rat or human origin cannot be distinguished by any known antibody. Therefore, confirming the human origin of myelin will depend on co-labeling with human markers. Multichannel confocal imaging (Figure 4B) and orthogonal projections (Figure 4C) show co-labeling of human fibers (hNCAM) with MBP (3D reconstruction in Figure 4D; Movie S1). Imaging of the paranodal and juxtaparanodal proteins that define the nodes of Ranvier demonstrates reduced density and loss of architecture following radiation, as is often reported in demyelination conditions (Uchida et al., 2012), but significant recovery after grafting (Figure 4E). 3D reconstruction of confocal optical sections showed the juxtaparanodal protein kv1.2 alternating with the paranodal protein Caspr1, in appropriate "paranodal" alignment along a myelinated fiber (Gu and Gu, 2011), with overlay of human NCAM, suggesting contribution of human cells to the reconstruction of a node of Ranvier (Figure 4F; Movie S2). Electron microscopy of brain sections showed areas of significant loss of myelin or degeneration and unraveling of the myelin sheath around the axons in the corpus callosum of the irradiated brains. In contrast, the grafted brains exhibited evidence of structural repair of the demyelinated areas with

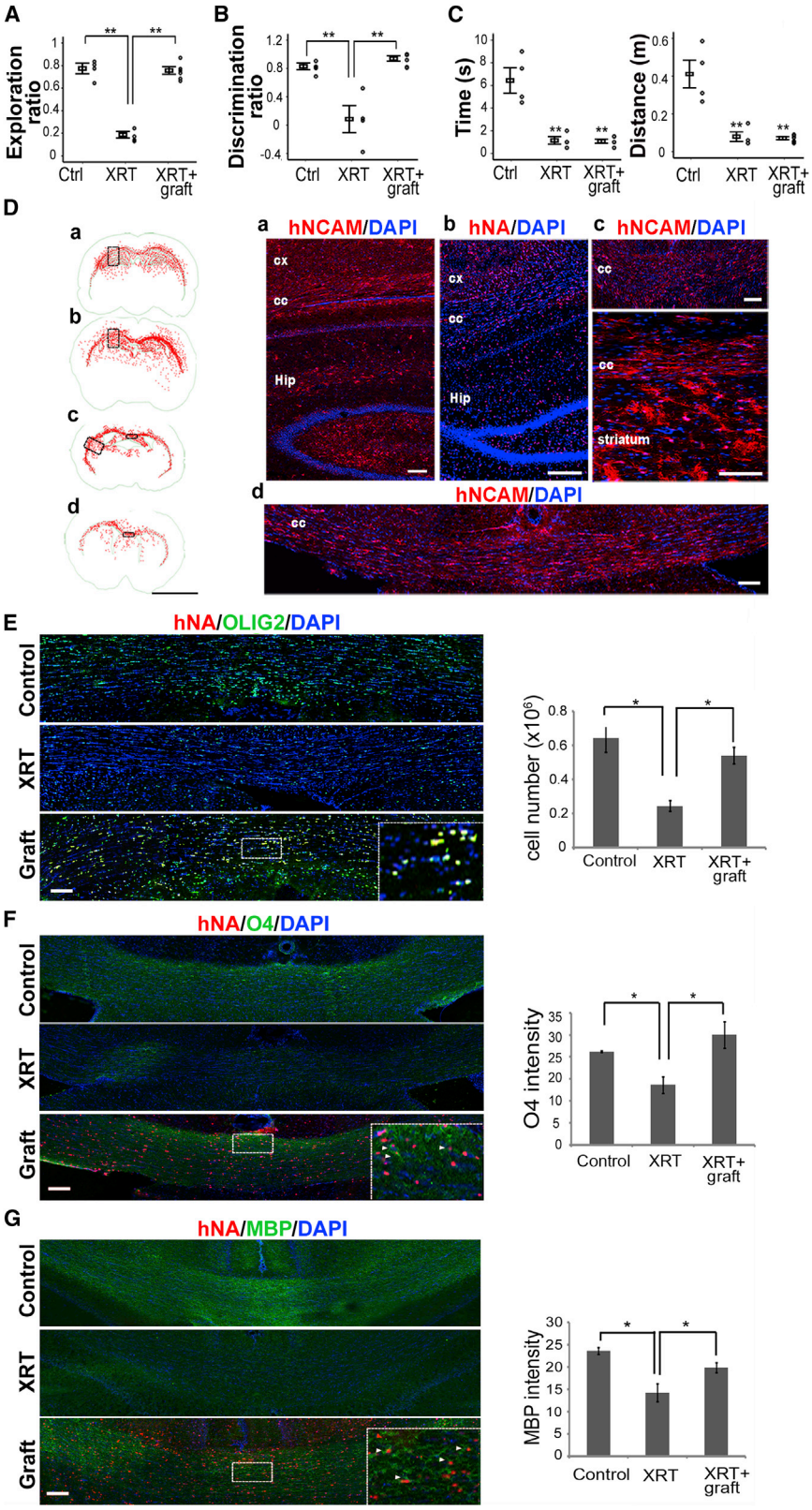

Figure 3. Grafted Human ES-Derived OPCs Remyelinate the Irradiated Brain and Ameliorate Cognitive Function

(A and B) Grafted animals (n = 6) showed significant improvement on the novel object preference (exploration ratio) and object location tasks (discrimination ratio) when compared to sham grafted irradiated animals (n = 4) to normal controls (n = 4).

(C) Grafted animals failed to improve on the rotarod task exhibiting scores that are similar to the irradiated sham injected group (XRT).

(D) Camera lucida representations of the distribution of human cells (marked by human nuclear antigen, hNA, or human NCAM [hNCAM]) in a series of coronal sections (a–d) of the brain; the cells migrate widely along white matter paths. Corresponding immunohistochemistry sections demonstrate the human cells in different regions. Cx, cortex; cc, corpus callosum; Hip, hippocampus. Scale bars represent 5 mm for the camera lucida; 100 μm for immunohistochemistry images.

(E) Immunohistochemistry (IHC) pictures and stereological calculation of the number of Olig2$^+$ cells in the corpus callosum of control, irradiated (XRT), and irradiated and grafted animals (Graft). Selected area of the grafted corpus callosum is shown in inset at higher magnification. Scale bar represents 100 μm.

(F and G) Representative IHC pictures and intensity quantification of O4 and MBP in the CC in control, XRT and XRT + graft rats. Selected areas of the grafted corpus callosum are shown in insets at higher magnification. Scale bar represents 100 μm.

All panels in (D)–(G) are composites of several low magnification images. All nuclei are counterstained in blue with DAPI. Data are reported as mean values ± SEM. (*$p < 0.05$. **$p < 0.01$). Circles (A)–(C) represent individual scores. See also Figures S4 and S6.

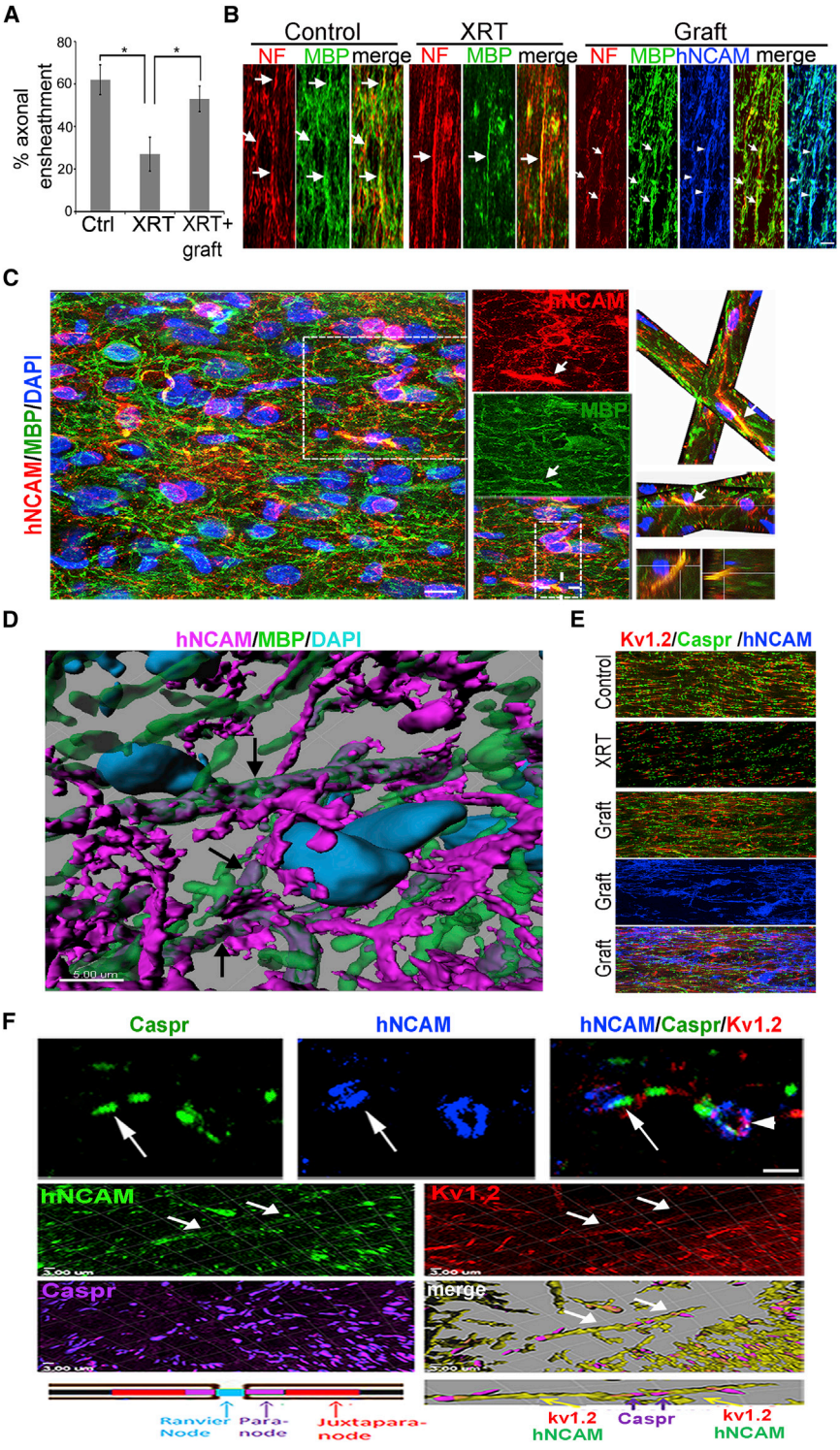

Figure 4. Quantification of Remyelination in the Grafted Irradiated Brains

(A) Quantification of axonal ensheathment demonstrates an increase in the percent myelinated axons after grafting. Data are reported as mean values ± SEM. *$p < 0.05$.

(B) Immunohistochemistry for MBP, neurofilament (NF), and human marker (hNCAM) shows colocalization of NF and MBP fibers and, in the graft group, additional co-labeling of MBP with hNCAM. The arrows point to myelinated axons (co-localization of MBP and NF) and the arrow heads indicate human myelin (co-localization with MBP and hNCAM). Scale bar represents 15 μm.

(C) Confocal imaging of human cells (identified with hNCAM) showing typical oligodendrocyte morphology co-labeled with MBP in cytoplasm and myelin sheath projections. Single channels are displayed in the middle panel, with white arrows identifying myelin from human origin. In the top right panel, two oblique slicers were used on the same field of view as the middle panel to confirm that MBP was expressed by hNCAM-expressing cells. In the right bottom panels, three-dimensional yz and xz orthogonal projections were shown to confirm MBP co-labeling with hNCAM (seen in yellow). Scale bar represents 10 μm.

(D) 3D reconstruction in high magnification of human graft cells projecting hNCAM labeled processes (magenta) that merge with MBP (green) along a probable axon in the cc. The MBP color was rendered semi-transparent to enhance visualization of the overlapping channels (arrows). Scale bar represents 500 μm. See also Movie S1.

(E) Representative confocal IHC images of junxtaparanodal protein kv1.2 and paranodal protein Caspr1 show restoration of nodal architecture in the grafted brain. Scale bar represents 15 μm.

(F) Triple labeling of sections of grafted irradiated brain with hNCAM, Caspr1 (arrows) and Kv1.2 (arrowheads), indicating that human cells associate closely with myelin fibers. Scale bar represents 10 μm. In the middle and lower panels, representative images show co-localization of hNCAM with the juxtaparanodal protein kv1.2 (merge as yellow) and alternating with host Caspr1 (magenta) in appropriate anatomic alignment, likely along a myelinated axon. In the lower right panel, 3D reconstruction performed with Bitplane Imaris software showing the structures in perspective. Scale bar represents 3 μm. The drawing in the lower left panel is a schematic representation to interpret the 3D model shown on the right side. See also Movie S2.

See also Figure S5.

recovery of thin yet compact myelin sheaths wrapped around healthy axons (Figure 5A). These findings are reflected in the quantification (Franklin and Ffrench-Constant, 2008) of the average g-ratio (0.70 in normal group, 0.76 in the XRT group and 0.72 in the XRT+ graft group; Figure 5B). Immunogold electron microscopy showed integration of human NCAM into the myelin sheaths and relatively rare immunogold particles that are not in association with myelin bundles (Figure 5C). Further quantification of myelination by the grafted cells was performed on IHC sections of MBP/hNCAM. The proportion of myelin of human origin in the grafted animals was calculated at ~47% (area of $hNCAM^+MBP^+/MBP^+$). Taken together, these data confirm

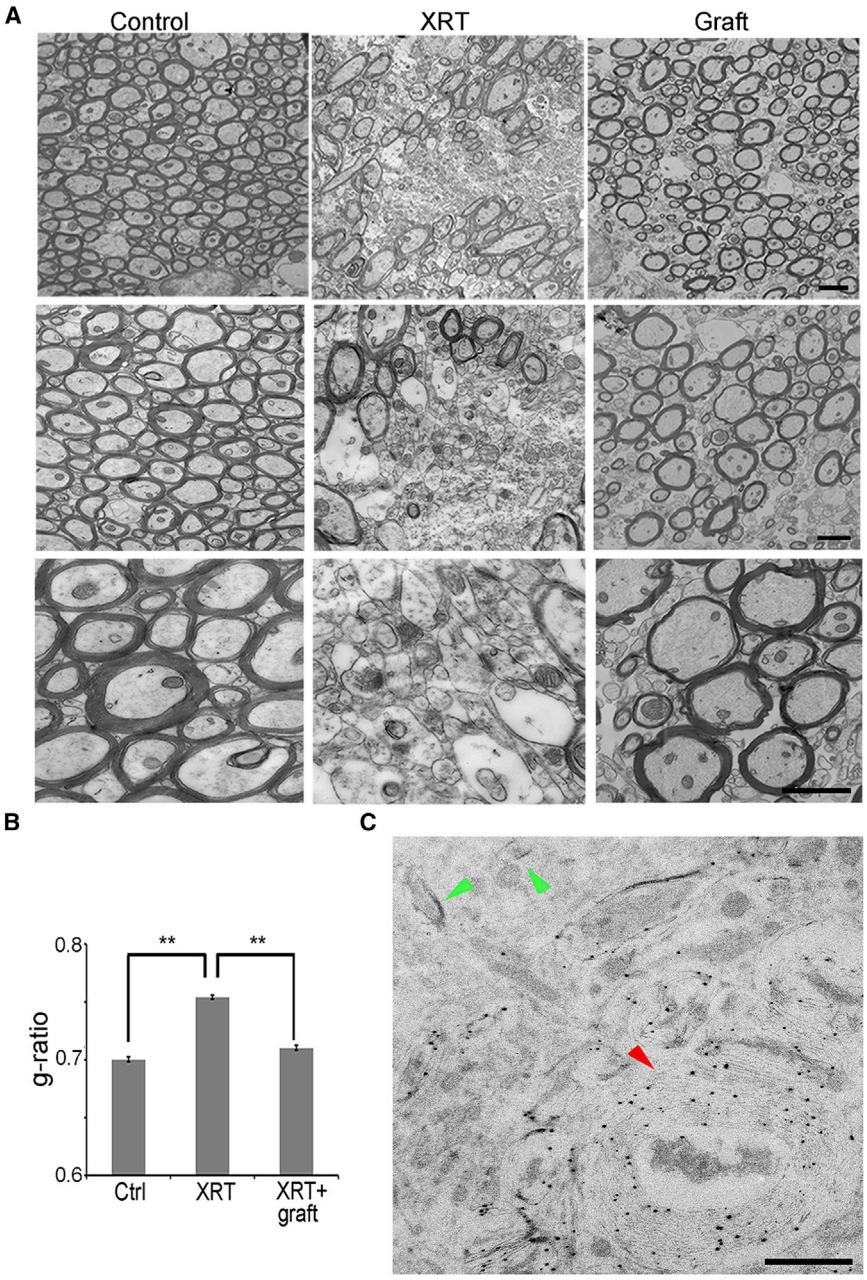

Figure 5. Ultrastructural Analysis of In Vivo Myelination by Human Grafts

(A) Representative EM images of the cc show patchy disruption of the myelin sheath around axons in the irradiated brain. The grafted brains show evidence of recovery of axonal myelination. Recent sheaths are thinner in diameter though they exhibit normal compact anatomy. Scale bar represents 2 μm in the upper panel and 500 nm for the two lower panels.

(B) g-ratios of the axons in corpus callosum in control, irradiated (XRT), and irradiated+graft (XRT+graft) groups. **p<0.01.

(C) Low power view of immuno-electron micrograph of hNCAM. The red arrowhead indicates myelin sheaths of an axonal projection with hNCAM gold labeling (10–25 nm black dots). Green arrows indicate endogenous myelin without immunolabeling. Scale bar represents 2 μm.

that grafted human cells extensively contribute to the structural and functional remyelination in the radiated brain. The transplanted cells did not promote astrogliosis or microglial/macrophage proliferation and activation (Figure S5C). Areas of neurogenesis such as the subventricular zone (SVZ) and hippocampus were impacted by radiation as reported in the literature (Romanko et al., 2004; Monje et al., 2002; Panagiotakos et al., 2007). Specifically there was a loss of doublecortin-expressing neuroblasts and proliferating cells (ki67) in the SVZ and hippocampus. Human cells were found in those regions but none exhibited neuronal differentiation, nor did they promote host-derived neurogenesis (Figures S5D and S5E). There was no evidence of teratomas or other signs of tumor formation, and no graft overgrowth was noted in any of the grafted animals. In fact, a phenotypic analysis of the cells did not demonstrate any Oct4, nestin, or Ki67 co-labeling with a human marker in the grafted brains (data not shown). Astrocytes of human origin were very rare, suggesting that the oligodendrocyte progenitors were either terminally committed or, less likely, that the microenvironment was not supportive of astrocytic differentiation. However, analysis of the cerebellum demonstrated complete absence of human cells and persistent demyelination (Figure S5F), thus possibly explaining the lack of improvement on the rotarod acceleration tasks.

Cerebellar Grafts Rescue Motor Coordination and Remyelinate the Cerebellum

A second group of animals (n = 28) was then subjected to the same radiation regimen, and received human ES-derived oligodendrocytes injected either in the cerebellum alone or in combination with the corpus callosum bilaterally. A total of 1 million cells were injected in the corpus callosum, as in the initial study. The cerebellum received a single injection of 250,000 $O4^+$ sorted cells in the central white matter. Animals were followed and tested behaviorally at two time points, 10 and 14 weeks post-injection. Performance on the novel object preference and object location tasks improved significantly in the group that received callosal and cerebellar grafts when compared to the non-transplanted animals, while the animals with grafts only in the cerebellum did not improve in any of the tests probing cognitive skills (Figure S6A). However, all grafted animals showed improvement in the rotarod task, including those that received cerebellar only injections (Figure 6A). Histological analysis of the brains demonstrated survival and migration of the human cells in the cerebellum (Figure 6B). There was also evidence of remyelination of the cerebellum in

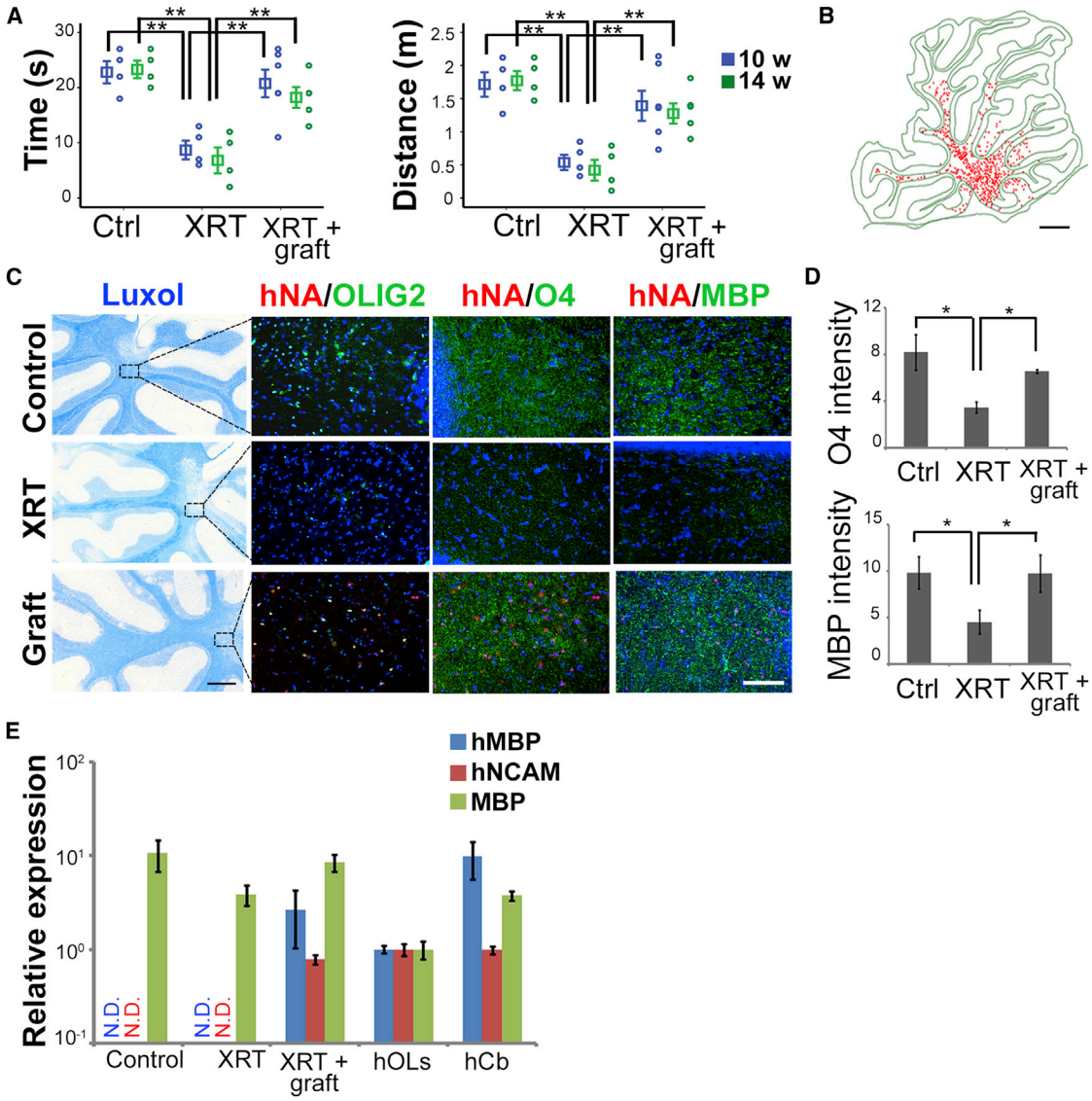

Figure 6. Cerebellar Grafts Rescue Motor Coordination and Remyelinate the Cerebellum

(A) Grafted animals showed improvement on the accelerating rotarod tasks (n = 6).

(B) Representative camera lucida illustration of the distribution of human cells in the cerebellum, detected by IHC for human nuclear antigen (hNA). Scale bar represents 1mm.

(C) Representative Luxol fast blue staining of sagittal sections of the cerebellum and IHC images showing myelin loss in the XRT group and recovery upon grafting. Human cells (hNA) co-label with olig2, O4, and MBP. Scale bar represents 0.5 mm in the luxol images and 100 μm in the IHC images.

(D) Quantification of O4 and MBP image intensity in the white matter of cerebellum.

(E) Human-specific MBP mRNA was detectable in the grafted group, as well as the human ESC-derived oligodendrocytes and the normal human cerebellum tissue (hCb). Expression levels of human NCAM and MBP (human and rat) mRNA are also analyzed as reference. The relative expression of mRNA was normalized to human OPCs. N.D., non detectable.

Data in (A), (D), and (E) are reported as mean values ± SEM with the indicated significance (*$p < 0.05$, **$p < 0.01$). See also Figure S6.

all grafted animals as assessed by Luxol histochemistry and quantitative immunofluorescence for olig2, O4, and MBP (Figures 6C and 6D). Animals that received cell injections in the cerebellum only did not exhibit remyelination in the corpus callosum or elsewhere in the cerebral hemispheres. There was no evidence for endogenous or human astrogliosis, excessive proliferation, or teratomas. To further support the role of human cell-mediated structural repair, we performed qRT-PCR to confirm the presence of myelin of human origin in the grafted tissue. The data demonstrate the expression of a human-specific MBP mRNA isoform in the grafted rat tissue, normal human cerebellum, and human ESC-derived oligodendrocytes, but not in the control or irradiated rat brains (Figure 6E). Expression of human NCAM and MBP (recognizing both human and rat) mRNA were also detected in the same samples as reference. These data provide strong evidence for structural repair of the

demyelinated irradiated brain via human ES-derived oligodendrocytes, leading to behavioral recovery that is specific to the remyelinated region of the brain.

DISCUSSION

As intense efforts in cancer therapies succeed in achieving long periods of remission and hopes of long-term survival, a focus on improving quality of life among survivors is more pressing. Radiation damage to the brain ranks among the major contributors to poor quality of life and is currently untreatable (Van Dongen-Melman et al., 1997; Yabroff et al., 2004). Here we demonstrate that remyelination of the irradiated brain via grafting of human oligoprogenitors can lead to cognitive and motor amelioration. Our model holds particular promise in view of the substantial and clinically relevant dose of fractionated radiation used, 50 Gy. There are reports of repair of radiation-induced demyelination, e.g., in the spinal cord, though the animal models used often received a single dose of radiation (Sun et al., 2013). Here we have focused on modeling whole-brain or large-volume radiation, rather than single high-dose focal radiation. Available clinical regimens are highly variable depending on the disease being treated. Commonly, whole-brain or large-volume partial brain radiation involves the delivery of 30–60 Gy in multiple fractions. It is difficult to fully mimic the human regimens. In particular, the dose per fraction we used is higher than average, largely due to logistical reasons, because the rodents have to be fully anesthesized for each dose of radiation.

Radiation injury is a complex phenomenon with a myriad of direct and indirect consequences, such as an impact on the vascular compartment, glia, local inflammatory systems, neurogenesis, and altered neuronal function (Bentzen, 2006; Greene-Schloesser et al., 2013). Recent reports have shown improvement of cognitive tasks following injection of neural stem cells in the hippocampus of irradiated rats, though the radiation regimen was subtherapeutic (Acharya et al., 2014). It is unclear to what extent rescue of hippocampal neurogenesis would contribute to symptom amelioration in humans. Despite the absence of neuronal differentiation by our cells and the decreased neurogenesis in the hippocampus following radiation, the animals exhibited improvement in cognition and in motor function, suggesting an important role for white matter recovery. The correlation of behavioral amelioration with the site of cell injection and area of remyelination support cell-mediated repair, though the possibility of a favorable paracrine role for the grafted cells cannot be completely excluded.

We also present a robust protocol for the derivation of highly enriched fully committed oligodendrocytes from human ESCs or iPSCs, capable of widespread migration and efficient myelination with near complete absence of other phenotypes and no evidence for proliferative cell types, primitive progeny, or teratomas. Such an approach can be fully GMP-compatible including the sorting step, though further acceleration of the in vitro period would be desirable. Pluripotent stem cells (PSC) are also an attractive cell source given their scalability, at the level of the undifferentiated cells which are readily expandable, as well as during the differentiation process. We estimate based on numerous replications of this protocol, that starting with 10 million undifferentiated hESCs (a few vials), we can obtain about 214 million well characterized $O4^+$ cells at day 100 of culture (assuming an $O4^+$ recovery rate of 35%). A main limiting factor for PSC-based cell therapies is often the ability to direct their differentiation into authentic and stable phenotypes. This is a particularly challenging task if the cells of interest develop late or need to be fully functional prior to transplantation. Here, we present a reliable differentiation strategy with stable phenotypes that closely resemble current definitions of oligodendrocyte progenitors (markers, gene-expression profile). In vivo, the overwhelming majority of the cells develops into mature myelinating oligodendrocytes or remains in the oligoprogenitor stage. We rarely identify any other phenotypes and there were no teratomas or areas of graft overgrowth, though assessments following longer in vivo periods, such as one year or longer, should be performed. Our strategy also includes a sorting step, which not only enriches for the phenotype of interest, but also presents an opportunity for indirectly selecting out undifferentiated ESCs, which are a source of safety concerns. A more aggressive negative selection approach can also be contemplated, but to our knowledge, it has not been a strict prerequisite for FDA approval of pluripotent stem cell based therapies. On the other hand, the differentiation protocol remains rather lengthy and will need to be optimized further for logistical purposes, if GMP manufacturing is planned.

Other human cell sources have been used successfully for remyelination in rodent models, such as fetal or adult white-matter progenitors (Windrem et al., 2004) though access to these cell sources can be difficult, especially because the cells need to be replenished because they are not highly expandable. The FDA has also approved early phase trials of multiply passaged multipotent neural stem cells isolated from fetal brain (Uchida et al., 2012; Gupta et al., 2012). These cells, manufactured to a clinical grade, have been used for a wide range of disorders (Pelizaeus-Merzbacher disease, neuronal ceroid lipofuscinosis, and spinal cord injury; see https://clinicaltrials.gov/). The cells are thought to provide a very beneficial neuroprotective effect.

The requirement for immunosuppression is another important issue in planning for clinical applications, though it remains the subject of debate. The preponderance of available data points towards the need for at least temporary immunosuppression at the time of surgical injection. The specific agents to be used and the total duration of treatment are also highly variable (Tadesse et al., 2014). In the case of radiation injury, immunosuppression could increase the burden of treatment-related morbidities, though most patients already receive far harsher chemotherapeutic agents. On the other hand, the derivation of engraftable oligoprogenitors from iPSCs is robust and feasible, as shown by our group and others; the majority of cancer patients can safely provide genetically normal somatic cells, such as skin, for iPS production, thereby developing a customized autologous cell source. However, there remain significant regulatory hurdles, as well as some scientific concerns, over the clinical use of iPSCs, despite their recent approval in Japan for the treatment of Parkinson's disease.

In summary, our results suggest that countering the cognitive side effects of radiation injury can be achieved safely, using human pluripotent cell-derived oligodendrocytes, thus paving the road towards a clinical trial for a condition that currently has no viable therapeutic options. The protocol could also be readily

adapted to other demyelination disorders and, although further long term data will be required, these results represent a robust first set of preclinical studies, with an eye towards future translation.

EXPERIMENTAL PROCEDURES

Animals, X-Irradiation, and Cell Transplantation

Female Athymic nude rats (RNU rat Crl:NIH-Foxn1rnu, Charles River Laboratories) aged 4 weeks were randomized into three age-matched groups: non-irradiated ("control" rats, n = 16 in total), irradiated rats with sham transplantation of HBSS (XRT, n = 17 in total), and irradiated rats transplanted with human ESC-derived OPCs (XRT + graft, n = 18 in total). Radiation was administered to the cranium using a 250 kV-orthovoltage system. Animals were anesthetized by ketamine (90 mg/kg)/xylazine (4 mg/kg) and placed on a custom-designed positioning platform covered with a protective lead plate with an adjustable aperture, which focuses the radiation delivery to the skull while shielding the rest of the body. A total dose of 50 Gy was administered in 10 fractions (5 Gy/fraction/day), over 2 weeks. One month after irradiation, human cells were transplanted into the corpus callosum, in 2 injections of 250,000 cells in each hemisphere, for a total of 1 million cells (Coordinates: AP −0.40 mm, ML −2.4 mm, VRT −3 mm; AP −0.40 mm, ML 2.4 mm, VRT −3 mm; AP −1.30 mm, ML –2 mm, VRT −3.2 mm; AP −1.30 mm, ML 2 mm, VRT −3.2 mm; tooth bar set at 0). Cerebellar injections were performed unilaterally into the cerebellar white matter and consisted of 250,000 cells delivered stereotactically (Coordinates: AP −12 mm, ML –0.9 mm, VRT −4.2 mm; tooth bar set at 0). The rats were anaesthetized with Ketamine/xylazine during the surgical procedures. Cells were delivered via a Hamilton Syringe (Hamilton Company) on a stereotactic Kopf frame (David Kopf Instruments). All animal procedures and care were performed according to NIH guidelines and following IACUC approval.

Human ESC-Derived Oligodendrocyte Precursor Cell Culture

Human ESCs (WA-09, XX, passages 35–45) were cultured on mouse embryonic fibroblasts (MEFs, GlobalStem) in medium of DMEM/F12 containing 20% knockout serum replacement (Gibco), 0.1 mM β-mercaptoethanol, and 6 ng/ml FGF-2 (R&D Systems). hESCs and iPSCs were used according to institutional ESCRO guidelines and approval.

Neural Induction

For neural induction, a modified version of the dual-SMAD inhibition was used. Undifferentiated hESCs were disaggregated using Accutase (Innovative Cell Technology) and plated on on Matrigel (BD Bioscience)-coated dishes at a density of 40,000 cells/cm2 in MEF conditioned hESC medium supplemented with 10 ng/ml of FGF-2 and Y-27632 (10μM, Tocris Bioscience). When the cells reached a confluent state (2–3 days after plating), they were exposed for 9 days to LDN193189 (200nM, Stemgent) and SB431542 (10 μM, Tocris) in knockout serum replacement medium (KSR) containing DMEM, 15% knockout serum replacement, 2 mM L-glutamine and 10 μM β-mercaptoethanol. Starting from day 5, Purmorphamine (1 μM, Stemgent) was added to differentiation media. KSR medium was gradually replaced with N2 medium (25%, 50%, 75%) starting on day 4 of differentiation as described previously (Chambers et al., 2009).

Patterning and Differentiation of Oligodendrocytes

On day 12, cells were dissociated using Accutase and replated in high-density conditions (300,000 cells per cm2) on dishes precoated with polyornithine (PO; 15 μg/ml), laminin (Lam; 1 μg/ml) and fibronectin (FN; 2 μg/ml) in N2 medium supplemented with brain-derived neurotrophic factor (BDNF; 20 ng/ml, R&D), ascorbic acid (AA; 0.2 mM, Sigma-Aldrich), Purmorphamine (1 uM, Stemgent) and fibroblast growth factor 8 (FGF8; 100 mg/ml, R&D). They are patterned at the P1 stage for 2 weeks. After two weeks of patterning, cells were passaged by mechanical picking of the CNS clusters and re-plated on PO/Lam/FN coated dishes (P2). Starting with P3, neural precursor cells (NPCs) were maintained in N2/B27 medium supplemented with Purmorphamine and FGF8 until day 40 when they were further exposed to glial media containing platelet-derived growth factor (PDGF; 20 ng/ml, R&D), insulin-like growth factor 1 (IGF-1; 20 ng/ml, R&D), triiodothyronine (T3; 20 ng/ml, Sigma-Aldrich) and dibutyryl cAMP (0.1 mM, Sigma-Aldrich). Medium was changed every 2 days, whereas the cultures were passaged every 2 weeks.

Microarray Analysis

For microarray analysis, total RNA from undifferentiated hESCs (control condition) and 70 days old, O4 sorted OPCs was collected using Trizol LS (Invitrogen). Samples were processed by the MSKCC Genomic core facility and hybridized on Illumina Human HT-12 Oligonucleotide arrays (total of 34,694 genes). Gene-expression analysis was done with the Partek Genomics Suite. Genes that had an adjusted p value < 0.05 and a fold change greater than two were considered significant. Raw data for the microarray gene expression reported in this study are available from the public repository of GEO Data Sets (accession number GSE63318). Top enriched gene groups were obtained using Gene Ontology enrichment analysis (DAVID) and are presented as a function of the corresponding Benjamini–Hochberg FDR corrected p values.

In Vitro Myelination Assay

hESC-derived neural stem cells were generated using a modified dual SMAD inhibition protocol (Chambers et al., 2009). Differentiation of neurons from NSCs was achieved by seeding the NSCs at low density in N2 medium without growth factors. Nearly homogenous populations of neurons were generated within 30 days and used for co-culture experiments. Hippocampal neurons were isolated from postnatal day 1 SD rats (Gardner et al., 2012).

Human ES-derived neuronal cells and rat hippocampal neurons were co-cultured with human PSC-derived OPCs sorted for O4 on poly-O-ornithine (50 μg/ml) and laminin (1μg/ml) coated wells in Neurobasal medium (Life Technologies) with B27 (Life Technologies), GlutaMAX-I Supplement (2 mM, Life Technologies), BDNF (20 ng/ml), AA (0.2 mM), T3 (60 ng/ml, Sigma-Aldrich), and cAMP (0.2 mM, Sigma-Aldrich) for 4 weeks and 5 weeks, respectively. Myelination was identified as co-labeling of SMI312 (axons) and MBP (oligodendrocyte processes). The length of axons was measured according to the method described by Deshmukh et al. (2013) with minor modifications. In our experiments, myelination was identified as regions of co-localization between MBP-positive oliogodendrocyte processes and SMI312-positive neuritis, and the length was measured with the NIH ImageJ software. This measurement was analyzed in ten randomly chosen fields from replicate co-culture samples. For the EM studies the co-cultures were maintained for 7 weeks. The differentiation medium was changed twice a week.

Behavioral Testing

We used the novel object-preference task and novel place-recognition tests, modified from Barker et al. (Barker et al., 2007). An open field arena (TSE Systems) was used for testing. During the testing, the time to explore the objects was recorded and analyzed by Videomot2 (TSE Systems). In brief, for novel object-preference task, rats were allowed to habituate twice in the arena with two identical objects for 5 minutes. Then the rats were placed in the arena for 3 minutes with one novel object and one familiar object. The data was presented as exploration ratio or ratio of time spent exploring the novel object versus both objects. For the object-location task, the rats were habituated to two identical objects for 10 minutes. Then they were placed in the arena with one object moved to a new location (novel place) and another identical object remaining in the same position (familiar place) for 3 minutes. The data was presented as discrimination ratio = (time exploring the object in the novel place − the familiar place) / time spent exploring both objects. The Morris water maze test was performed as described by Vorhees et al. (Vorhees and Williams, 2006). An automated rotarod treadmill (7 cm diameter rod, IITC Life Science Inc.) was used in the rotarod analysis. The rats were pre-trained to learn to run on a rotating rod at 5 rpm and 10 rpm prior to testing. The rotarod was accelerated from 15 to 40 rpm over 60 seconds for the analysis. The length of time and distance traveled until the rats fell off the rod were recorded.

Statistics

Results are expressed as the mean ± SEM. The statistical analysis was performed using IBM SPSS Statistics (version 21) software. Normality was tested by Shapiro-Wilk test. Statistical analysis was performed by ANOVA. Homogeneity of variance was tested. $p \leq 0.05$ was considered to denote significance.

ACCESSION NUMBERS

The GEO accession number for the microarray data reported in this paper is GSE63318.

SUPPLEMENTAL INFORMATION

Supplemental Information includes six figures, Supplemental Experimental Procedures, and two movies and can be found with this article online at http://dx.doi.org/10.1016/j.stem.2015.01.004.

AUTHOR CONTRIBUTIONS

J.P. conducted all the in vivo experiments, supervised and/or performed the behavior tests, assisted with the EM images, and co-wrote the manuscript; T.M. conducted all the in vitro studies and co-wrote parts of the manuscript. G.A. and E.P. assisted with behavioral testing and radiation experiments; J.M. and L.D. performed many technical tasks; P.G. consulted on overall plans and experimental design; K.U. performed and /or supervised the EM experiments; J.T. provided the hES derived neurons; D.S. assisted with confocal imaging, 3D rendering, animations, and graphics; and V.T. contributed to overall plan, experimental design and setups, data interpretation, and manuscript writing.

ACKNOWLEDGMENTS

The work was supported by a grant from the NINDS (R01NS054009), the New York State Stem Cell Board (NYSTEM), and the Tri-Institutional Stem Cell Initiative (Tri-Sci). T.M. was supported in part by a Fellowship from the Tri-Sci. D.S. is a Research Scholar from Le Fonds de Recherche du Québec - Santé (FRQ-S) and holds a Junior 1 Career Award. We would like to thank Alexander Lucaci and Rebecca Chen for help with the behavior experiments, Tom Losasso with the radiation dosimetry, Katia Manova, Vitaly Boyko, Fujisawa Sho, and Ke Xu at the Molecular Cytology Core Facility, and Nina Lampen at The Electron Microscopy facility, all at Memorial Sloan Kettering Cancer Center. We are grateful to William Stallcup for the gift of PDGFRα antibody and to Steve Goldman for O4 antibody aliquots.

Received: December 15, 2013
Revised: November 24, 2014
Accepted: January 13, 2015
Published: February 5, 2015

REFERENCES

Acharya, M.M., Christie, L.-A., Hazel, T.G., Johe, K.K., and Limoli, C.L. (2014). Transplantation of human fetal-derived neural stem cells improves cognitive function following cranial irradiation. Cell Transplant. *23*, 1255–1266.

Antunes, M., and Biala, G. (2012). The novel object recognition memory: neurobiology, test procedure, and its modifications. Cogn. Process. *13*, 93–110.

Barker, G.R.I., Bird, F., Alexander, V., and Warburton, E.C. (2007). Recognition memory for objects, place, and temporal order: a disconnection analysis of the role of the medial prefrontal cortex and perirhinal cortex. J. Neurosci. *27*, 2948–2957.

Bentzen, S.M. (2006). Preventing or reducing late side effects of radiation therapy: radiobiology meets molecular pathology. Nat. Rev. Cancer *6*, 702–713.

Chambers, S.M., Fasano, C.A., Papapetrou, E.P., Tomishima, M., Sadelain, M., and Studer, L. (2009). Highly efficient neural conversion of human ES and iPS cells by dual inhibition of SMAD signaling. Nat. Biotechnol. *27*, 275–280.

Deshmukh, V.A., Tardif, V., Lyssiotis, C.A., Green, C.C., Kerman, B., Kim, H.J., Padmanabhan, K., Swoboda, J.G., Ahmad, I., Kondo, T., et al. (2013). A regenerative approach to the treatment of multiple sclerosis. Nature *502*, 327–332.

Douvaras, P., Wang, J., Zimmer, M., Hanchuk, S., O'Bara, M.A., Sadiq, S., Sim, F.J., Goldman, J., and Fossati, V. (2014). Efficient generation of myelinating oligodendrocytes from primary progressive multiple sclerosis patients by induced pluripotent stem cells. Stem Cell Reports *3*, 250–259.

Duffner, P.K., Cohen, M.E., Thomas, P.R., and Lansky, S.B. (1985). The long-term effects of cranial irradiation on the central nervous system. Cancer *56*, 1841–1846.

Franklin, R.J.M., and Ffrench-Constant, C. (2008). Remyelination in the CNS: from biology to therapy. Nat. Rev. Neurosci. *9*, 839–855.

Gardner, A., Jukkola, P., and Gu, C. (2012). Myelination of rodent hippocampal neurons in culture. Nat. Protoc. *7*, 1774–1782.

Gibbs, I.C., Tuamokumo, N., and Yock, T.I. (2006). Role of radiation therapy in pediatric cancer. Hematol. Oncol. Clin. North Am. *20*, 455–470.

Greene-Schloesser, D., Robbins, M.E., Peiffer, A.M., Shaw, E.G., Wheeler, K.T., and Chan, M.D. (2012). Radiation-induced brain injury: A review. Front Oncol *2*, 73.

Greene-Schloesser, D., Moore, E., and Robbins, M.E. (2013). Molecular pathways: radiation-induced cognitive impairment. Clin. Cancer Res. *19*, 2294–2300.

Gu, C., and Gu, Y. (2011). Clustering and activity tuning of Kv1 channels in myelinated hippocampal axons. J. Biol. Chem. *286*, 25835–25847.

Gupta, N., Henry, R.G., Strober, J., Kang, S.M., Lim, D.A., Bucci, M., Caverzasi, E., Gaetano, L., Mandelli, M.L., Ryan, T., et al. (2012). Neural stem cell engraftment and myelination in the human brain. Sci Transl Med. *4*, 155ra137.

Harauz, G., and Boggs, J.M. (2013). Myelin management by the 18.5-kDa and 21.5-kDa classic myelin basic protein isoforms. J. Neurochem. *125*, 334–361.

Hu, B.Y., Du, Z.W., Li, X.J., Ayala, M., and Zhang, S.C. (2009). Human oligodendrocytes from embryonic stem cells: conserved SHH signaling networks and divergent FGF effects. Development *136*, 1443–1452.

Kurita, H., Kawahara, N., Asai, A., Ueki, K., Shin, M., and Kirino, T. (2001). Radiation-induced apoptosis of oligodendrocytes in the adult rat brain. Neurol. Res. *23*, 869–874.

Mabbott, D.J., Noseworthy, M.D., Bouffet, E., Rockel, C., and Laughlin, S. (2006). Diffusion tensor imaging of white matter after cranial radiation in children for medulloblastoma: correlation with IQ. Neuro-oncol. *8*, 244–252.

Miller, J.D., Ganat, Y.M., Kishinevsky, S., Bowman, R.L., Liu, B., Tu, E.Y., Mandal, P.K., Vera, E., Shim, J.W., Kriks, S., et al. (2013). Human iPSC-based modeling of late-onset disease via progerin-induced aging. Cell Stem Cell *13*, 691–705.

Monje, M.L., Mizumatsu, S., Fike, J.R., and Palmer, T.D. (2002). Irradiation induces neural precursor-cell dysfunction. Nat. Med. *8*, 955–962.

Monje, M.L., Toda, H., and Palmer, T.D. (2003). Inflammatory blockade restores adult hippocampal neurogenesis. Science *302*, 1760–1765.

Oi, S., Kokunai, T., Ijichi, A., Matsumoto, S., and Raimondi, A.J. (1990). Radiation-induced brain damage in children—histological analysis of sequential tissue changes in 34 autopsy cases. Neurol. Med. Chir. (Tokyo) *30*, 36–42.

Panagiotakos, G., Alshamy, G., Chan, B., Abrams, R., Greenberg, E., Saxena, A., Bradbury, M., Edgar, M., Gutin, P., and Tabar, V. (2007). Long-term impact of radiation on the stem cell and oligodendrocyte precursors in the brain. PLoS ONE *2*, e588.

Paumier, A., Cuenca, X., and Le Péchoux, C. (2011). Prophylactic cranial irradiation in lung cancer. Cancer Treat. Rev. *37*, 261–265.

Ringborg, U., Bergqvist, D., Brorsson, B., Cavallin-Ståhl, E., Ceberg, J., Einhorn, N., Frödin, J.-E., Järhult, J., Lamnevik, G., Lindholm, C., et al. (2003). The Swedish Council on Technology Assessment in Health Care (SBU) systematic overview of radiotherapy for cancer including a prospective survey of radiotherapy practice in Sweden 2001—summary and conclusions. Acta Oncol. *42*, 357–365.

Romanko, M.J., Rola, R., Fike, J.R., Szele, F.G., Dizon, M.L., Felling, R.J., Brazel, C.Y., and Levison, S.W. (2004). Roles of the mammalian subventricular zone in cell replacement after brain injury. Prog. Neurobiol. *74*, 77–99.

Sano, K., Morii, K., Sato, M., Mori, H., and Tanaka, R. (2000). Radiation-induced diffuse brain injury in the neonatal rat model—radiation-induced

apoptosis of oligodendrocytes. Neurol. Med. Chir. (Tokyo) *40*, 495–499, discussion 499–500.

Saxe, M.D., Battaglia, F., Wang, J.-W., Malleret, G., David, D.J., Monckton, J.E., Garcia, A.D., Sofroniew, M.V., Kandel, E.R., Santarelli, L., et al. (2006). Ablation of hippocampal neurogenesis impairs contextual fear conditioning and synaptic plasticity in the dentate gyrus. Proc. Natl. Acad. Sci. USA *103*, 17501–17506.

Schatz, J., Kramer, J.H., Ablin, A., and Matthay, K.K. (2000). Processing speed, working memory, and IQ: a developmental model of cognitive deficits following cranial radiation therapy. Neuropsychology *14*, 189–200.

Sun, Y., Xu, C.C., Li, J., Guan, X.Y., Gao, L., Ma, L.X., Li, R.X., Peng, Y.W., and Zhu, G.P. (2013). Transplantation of oligodendrocyte precursor cells improves locomotion deficits in rats with spinal cord irradiation injury. PLoS ONE *8*, e57534.

Tabar, V., and Studer, L. (2014). Pluripotent stem cells in regenerative medicine: challenges and recent progress. Nat. Rev. Genet. *15*, 82–92.

Tadesse, T., Gearing, M., Senitzer, D., Saxe, D., Brat, D.J., Bray, R., Gebel, H., Hill, C., Boulis, N., Riley, J., et al. (2014). Analysis of graft survival in a trial of stem cell transplant in ALS. Ann Clin Transl Neurol *1*, 900–908.

Uchida, N., Chen, K., Dohsa, M., Hansen, K.D., Dean, J., Buser, J.R., Riddle, A., Beardsley, D., Wan, Y., Gong, X., et al. (2012). Human neural stem cells induce functional myelination in mice with severe dysmyelination. Sci. Transl. Med. *4*, 155ra136.

Uh, J., Merchant, T.E., Li, Y., Feng, T., Gajjar, A., Ogg, R.J., and Hua, C. (2013). Differences in brainstem fiber tract response to radiation: a longitudinal diffusion tensor imaging study. Int. J. Radiat. Oncol. Biol. Phys. *86*, 292–297.

Van Dongen-Melman, J.E., De Groot, A., Van Dongen, J.J., Verhulst, F.C., and Hählen, K. (1997). Cranial irradiation is the major cause of learning problems in children treated for leukemia and lymphoma: a comparative study. Leukemia *11*, 1197–1200.

Vorhees, C.V., and Williams, M.T. (2006). Morris water maze: procedures for assessing spatial and related forms of learning and memory. Nat. Protoc. *1*, 848–858.

Wang, S., Bates, J., Li, X., Schanz, S., Chandler-Militello, D., Levine, C., Maherali, N., Studer, L., Hochedlinger, K., Windrem, M., and Goldman, S.A. (2013). Human iPSC-derived oligodendrocyte progenitor cells can myelinate and rescue a mouse model of congenital hypomyelination. Cell Stem Cell *12*, 252–264.

Windrem, M.S., Nunes, M.C., Rashbaum, W.K., Schwartz, T.H., Goodman, R.A., McKhann, G., 2nd, Roy, N.S., and Goldman, S.A. (2004). Fetal and adult human oligodendrocyte progenitor cell isolates myelinate the congenitally dysmyelinated brain. Nat. Med. *10*, 93–97.

Yabroff, K.R., Lawrence, W.F., Clauser, S., Davis, W.W., and Brown, M.L. (2004). Burden of illness in cancer survivors: findings from a population-based national sample. J. Natl. Cancer Inst. *96*, 1322–1330.